Chapter 16
Bond-Graph Modelling and Causal Analysis of Biomolecular Systems

Peter J. Gawthrop

16.1 Introduction

Bond graphs were introduced by Paynter [32] and their engineering application is described in number of textbooks [15, 21, 25, 44] and a tutorial for control engineers [10]. Bond graphs were first used to model chemical reaction networks by Oster et al. [28] and a detailed account is given by Oster et al. [29]. Subsequent to this, the bond graph approach to chemical reactions has been extended by Cellier [7], Thoma and Mocellin [42] and Greifeneder and Cellier [16]. In 1993, the inventor of bond graphs, Henry Paynter, said [33][1]:

> Katchalsky's breakthroughs in extending bond graphs to biochemistry are very much on my own mind. I remain convinced that BG models will play an increasingly important role in the upcoming century, applied to chemistry, electrochemistry and biochemistry, fields whose practical consequences will have a significance comparable to that of electronics in this century. This will occur both in device form, say as chemfets, biochips, etc., as well as in the basic sciences of biology, genetics, etc.

Based on the work of Katchalsky and coworkers [28, 29], and the more recent work of Gawthrop and Crampin [11, 12] and Gawthrop et al. [13], this chapter presents an introduction to the bond graph modelling of the biomolecular systems of living organisms. In particular, the approach is based on the transduction of Gibbs energy and the corresponding chemical potential/molar flow covariables appropriate to isothermal and isobaric thermodynamic systems [3, 5]. Molecular species are represented by non-linear **C** components and reactions by non-linear two-port

[1]This was pointed out to me by the Editor of this volume, Wolfgang Borutzky.

P.J. Gawthrop (✉)
Systems Biology Laboratory, Melbourne School of Engineering, University of Melbourne, Melbourne, VIC 3010, Australia
e-mail: peter.gawthrop@unimelb.edu.au

W. Borutzky (ed.), *Bond Graphs for Modelling, Control and Fault Diagnosis of Engineering Systems*, DOI 10.1007/978-3-319-47434-2_16

R components. As living systems are neither at thermodynamic equilibrium nor closed, open and non-equilibrium systems are considered and illustrated using examples of biomolecular systems. The bond graph representation of biomolecular systems is complicated by the fact that the **R** and **C** components are fundamentally nonlinear; however the bond graph representation of biomolecular systems is simplified by the fact that there are no **I** or **GY** components.

In addition to their role in ensuring that models are energetically correct, bond graphs provide a powerful and natural way of representing and analysing *causality*. Causality is used in this chapter to examine the properties of the junction structures of biomolecular systems. Junction structures define the behaviour of the systems and thus the analysis of junction structures can reveal hidden information about a biomolecular system. Ort and Martens [26] and Perelson [34] give a basic analysis of junction structures and Sueur and Dauphin-Tanguy [38, 39, 40] show how basic system properties such as structural controllability can be derived from the bond graph junction structure by applying both integral and derivative causality.

For the purposes of simulating a biomolecular system, the **C** components are all in integral causality. As will be seen in this chapter, different causal patterns can be used to probe the fundamental properties of the junction structure. Stoichiometric analysis of biomolecular systems [18, 22, 30, 31] looks at the null spaces of the *stoichiometric matrix* to derive fundamental properties of the systems expressed as *conserved moieties*[2] and *flux paths*. This chapter shows how these results are related to the causal properties of the bond graph junction structure and provides new insights into the dynamics of biomolecular systems.

Section 16.2 introduces bond graph modelling of biomolecular systems and Sect. 16.3 describes structural analysis of biomolecular systems using the junction structure concept. Section 16.4 gives a bond graph model of a classical biomolecular cycle described by Hill [17] and provides a junction structure based analysis of the system. Section 16.5 gives a bond graph model of a simplified model of glycolysis, an important component of the metabolism of living systems. Section 16.6 gives similar modelling and analysis of a key component of living systems: the phosphorylation/dephosphorylation reaction system. Section 16.7 contains concluding remarks and suggestions for further work.

16.2 Bond Graph Modelling of Biomolecular Systems

Section 16.2.1 gives some background thermodynamics based on the textbook of Atkins and de Paula [3]. Following the exposition of Gawthrop and Crampin [11], Sect. 16.2.2 defines the pair of energy covariables used for biomolecular modelling: chemical potential and molar flow rate. Section 16.2.3 looks at the bond graph **C**

[2]In this context, a *moiety* is a part of a molecule; in some reactions, such moieties are *conserved* across different molecules.

component which, in this context, corresponds to a chemical species. The effort variable is chemical potential which is also discussed by Fuchs [9] and Job and Herrmann [19]. Section 16.2.4 looks at the two-port **R** component (given the special name **Re** here) introduced by Oster et al. [29] to model a chemical reaction. A one-port **R** with associated **1** junction is also used to model reactions as discussed by Karnopp [20]. The corresponding effort variable is *affinity*, the weighted sum of chemical potentials, and the flow variable is molar flow. As discussed by Oster et al. [28, 29] and Gawthrop and Crampin [11] it is possible to model biomolecular systems without the use of inertial **I** or gyrator **GY** components. Some fundamental ideas related to this point are discussed by Breedveld [6].

The discussion here is restricted to single-compartment systems and a simple illustrative example is given in Sect. 16.2.5.

16.2.1 Basic Thermodynamics

The following definitions and results are drawn from [3, Sect. F2]; the adjectives *isobaric* and *isothermal* mean constant pressure and temperature respectively.

Molar amount. The number of moles n_A of a substance A is the ratio of the number of entities N_A to the Avogadro constant N_{Avo}

$$n_A = \frac{N_A}{N_{\text{Avo}}} \,\text{mol} \tag{16.1}$$

Mole fraction. In a mixture of substances the mole fraction χ_A[3] of substance A is the ratio of the molar amount n_A of A to the total molar amount of all substances in the mixture n_{total}

$$\chi_A = \frac{n_A}{n_{\text{total}}} \tag{16.2}$$

By definition: $0 \leq \chi_A \leq 1$.

Molar concentration. In a mixture of substances the molar concentration $[A]$ of substance A is the ratio of the molar amount n_A of A to the total volume $V_{\text{total}}\,\text{m}^3$

$$[A] = \frac{n_A}{V_{\text{total}}} \,\text{mol}\,\text{m}^{-3} \tag{16.3}$$

Confusingly, the symbol $[A]$ is also used to represent the non-dimensional quantity

$$\frac{[A]}{c^{\varnothing}} = \frac{n_A}{Vc^{\varnothing}} = \frac{\chi_A n_{\text{total}}}{Vc^{\varnothing}} \tag{16.4}$$

where $c^{\varnothing}$ is the standard concentration of $1\,\text{mol}\,\text{dm}^{-3}$.

[3]The standard notation would be x_A but this clashes with our bond graph notation.

Molar volume. The molar volume V_A of substance A is the volume that it occupies per mole

$$V_A = \frac{V_{\text{total}}}{n_A} \,\text{m}^3\,\text{mol}^{-1} \tag{16.5}$$

Gibbs energy. The Gibbs energy $G\,\text{J}$ (also called Gibbs free energy or just free energy) is defined as in terms of enthalpy $H\,\text{J}$, temperature $T\,\text{K}$ and entropy $S\,\text{J}\,\text{K}^{-1}$ as

$$G = H - TS\,\text{J} \tag{16.6}$$

Molar enthalpy. The molar enthalpy[4] H_A of substance A is the enthalpy per mole

$$H_A = \frac{H}{n_A} \,\text{J}\,\text{mol}^{-1} \tag{16.7}$$

Partial molar property. A partial molar property of a substance A forming part of a mixture is the contribution of that (extensive) property to the overall property of the mixture. The partial molar property depends not only on the substance but also on the other substances forming the mixture.

Chemical potential. The *partial* molar Gibbs energy of substance A is given the evocative title of *chemical potential* μ_A

$$\mu_A = G_{Am} = \frac{G_m}{n_A} \,\text{J}\,\text{mol}^{-1} \tag{16.8}$$

where G_m is the Gibbs energy of A within the current mixture. Alternatively, μ_A may be defined as $\frac{\partial G}{\partial n_A}$ where G is the total Gibbs energy of the mixture.[5]

Entropy exchange. When the *enthalpy* of an *isobaric system* changes by $\Delta H\,\text{J}$, the *entropy* of the *environment* $S_{\text{env}}\,\text{J}\,\text{K}^{-1}$ (assumed to be infinite and at a constant temperature T) changes by

$$\Delta S_{\text{env}} = -\frac{\Delta H}{T} \,\text{J}\,\text{K}^{-1} \tag{16.9}$$

Total entropy. If the system is isothermal (temperature $T\,\text{K}$) and isobaric, the total entropy change ΔS_{total} is given by

$$\Delta S_{\text{total}} = \Delta S - \frac{\Delta H}{T} \tag{16.10}$$

[4] Other extensive quantities such as internal energy, entropy, Gibbs energy also have molar versions.

[5] Michael Pan, private communication.

Change in Gibbs energy. For isothermal (temperature T K) and isobaric systems

$$\Delta G = \Delta H - T\Delta S = -T\Delta S_{\text{total}}\,\text{J} \tag{16.11}$$

Chemical potential of substance in an ideal solution. If Henry's law holds (equivalent to a dilute solution) and substance A is dilute

$$\mu_A = \mu_A^\star + RT \ln \chi_A\,\text{J mol}^{-1} \tag{16.12}$$

where μ_A is the chemical potential of A, χ_A is the mole fraction of A (16.2) and $\mu_A^\star$ is the value of μ_A when it is pure ($\chi_A = 1$). Defining x_A as the number of moles of substance A:

$$x_A = n_A\,\text{mol} \tag{16.13}$$

and x_{total} as the total number of moles of all substances in the mixture, Eq. (16.12) becomes

$$\mu_A = \mu_A^\star + RT \ln \frac{x_A}{x_{\text{total}}}\,\text{J mol}^{-1} \tag{16.14}$$

It is convenient to reformulate Eq. (16.14) as

$$\mu_A = RT \ln K_A x_A\,\text{J mol}^{-1} \tag{16.15}$$

$$\text{where } K_A = \frac{\exp \frac{\mu_A^\star}{RT}}{x_{\text{total}}}\,\text{mol}^{-1} \tag{16.16}$$

16.2.2 Bond Graph Covariables

This chapter considers isothermal isobaric systems. In this context, an appropriate pair of energy covariables for substance A is

Effort. Chemical potential μ as expressed in Eq. (16.15) with units of J mol^{-1}.
Flow. Molar flow rate v with units of mol s^{-1}.

The product of the effort and flow variables is $p = \mu v$ with units of J s^{-1} or W.

16.2.3 The Bond Graph C Component

The **C** component has one port with flow variable $v\,\text{mol s}^{-1}$ and associated effort variables the chemical potential $\mu\,\text{J mol}^{-1}$ given by Eq. (16.15). The component

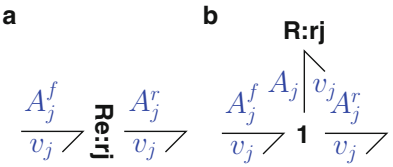

Fig. 16.1 Reaction component. (**a**) The **Re**:**rj** component relates the jth reaction flow rate v_j to the forward A_j^f and reverse A_j^r affinities. (**b**) The simplified version emphasises the common flow rate v_j by using the single port **R**:**rj** and the net affinity $A_j = A_j^f - A_j^r$

state $x_A = n_A$, the number of moles of substance A. Thus for substance A the corresponding **C** component has the equations

$$\dot{x}_A = v \qquad \text{mol s}^{-1} \tag{16.17}$$

$$\mu_A = RT \ln K_A x_A \,\text{J mol}^{-1} \tag{16.18}$$

The sole parameter is the *thermodynamic constant* K_A given by Eq. (16.16) with units of mol^{-1}; thus the argument of $K_A x_A$ of ln is dimensionless. The constant RT has units of J mol^{-1}.

16.2.4 The Bond Graph **Re** *Component*

The jth **Re** component of Fig. 16.1a has two ports with a common flow variable v_j and the associated effort variables are the forward and backward affinities A_j^f and A_j^r. As discussed by Gawthrop and Crampin [11] and based on the work of Van Rysselberghe [43] and Oster et al. [29, Sect. 5.1], the molar flow (or reaction rate) v_j is given by the *Marcelin–de Donder formula* in terms of A^f and A^r by

$$v_j = v_j^+ - v_j^- \tag{16.19}$$

$$\text{where } v_j^+ = \kappa_j e^{\frac{A_j^f}{RT}} \qquad \text{and} \qquad v_j^- = \kappa_j e^{\frac{A_j^r}{RT}} \tag{16.20}$$

where the *reaction constant* $\kappa_j \geq 0$. The exponential term in Eq. (16.19) of the **Re** component, coupled with the logarithmic term in Eq. (16.18) of the **C** component gives rise to sums of states being converted into products of states and gives rise to the *mass-action* form of the reaction flows.

An **Re** component with net affinity $A_j = A_j^f - A_j^r$ and molar flow v_j dissipates Gibbs energy at a rate $\dot{G}_j$ given by

$$\dot{G}_j = v_j \left(A_j^f - A_j^r\right) = \left(v_j^+ - v_j^-\right)\left(A_j^f - A_j^r\right) \tag{16.21}$$

Note that when $A_j = 0$ both $v_j = 0$ and $\dot{G}_j = 0$. Thus, to show that **Re** is dissipative, it is necessary to show that $\dot{G}_j$ is positive for all $v_j \neq 0$.

Using Eq. (16.20)

$$A_j^f = RT \ln \frac{v_j^+}{\kappa_j} \qquad \text{and} \qquad A_j^r = RT \ln \frac{v_j^-}{\kappa_j} \tag{16.22}$$

$$\text{and so } \dot{G}_j = RT \left(v_j^+ - v_j^- \right) \ln \frac{v_j^+}{v_j^-} \tag{16.23}$$

Equation (16.23) is given by Qian and Beard [36, Eq. (5)] and Polettini and Esposito [35].

From Eq. (16.20), both v_j^+ and v_j^- are positive and so it is possible to write $v_j^+ = \rho v_j^-$ where ρ is positive. Hence Eq. (16.23) can be rewritten as

$$\dot{G}_j = RT v_j^- (\rho - 1) \ln \rho \tag{16.24}$$

There are three possibilities: if $\rho > 1$ then both $(\rho - 1) > 0$ and $\ln \rho > 0$ and so, as $v_j^- > 0$, $\dot{G}_j > 0$; if $\rho < 1$ then both $(\rho - 1) < 0$ and $\ln \rho < 0$ and so, as $v_j^- > 0$, $\dot{G}_j > 0$; and, if $\rho = 1$, both $(\rho - 1) = 0$ and $\ln \rho = 0$ and $\dot{G}_j = 0$. Hence if $v_j \neq 0$, $\dot{G}_j > 0$ and if $v_j = 0$, $\dot{G}_j = 0$.

From Eqs. (16.10) and (16.11), the *enthalpy* dissipated by the resistor reappears as external *entropy* and the remainder of the Gibbs energy ($T\Delta S$) represents a change of internal entropy. Thus only the enthalpy portion of the Gibbs energy is dissipated as "heat of reaction"—more properly called enthalpy of reaction. This phenomenon has been called *entropy stripping* [41, 42].

The two ports of the reaction component **Re** of Fig. 16.1a are needed to separately convey the affinities A_j^f and A_j^r to Eq. (16.19). However, as pointed out by Karnopp [20], the one port **R** and **1** junction version of Fig. 16.1b more clearly shows that the molar flow v_j is common to both ports and thus mass is conserved. The **R** component can be suitably modulated to have the same effect as the **Re** component. The one port version of Fig. 16.1b will be used for the structural analysis of Sect. 16.3.

16.2.5 Example

Figure 16.2a corresponds to a biomolecular system with three species (A, B, C) and three reactions ($r1$, $r2$, $r3$) given by the chemical formulae

$$A \overset{1}{\rightleftharpoons} B \overset{2}{\rightleftharpoons} C \overset{3}{\rightleftharpoons} A \tag{16.25}$$

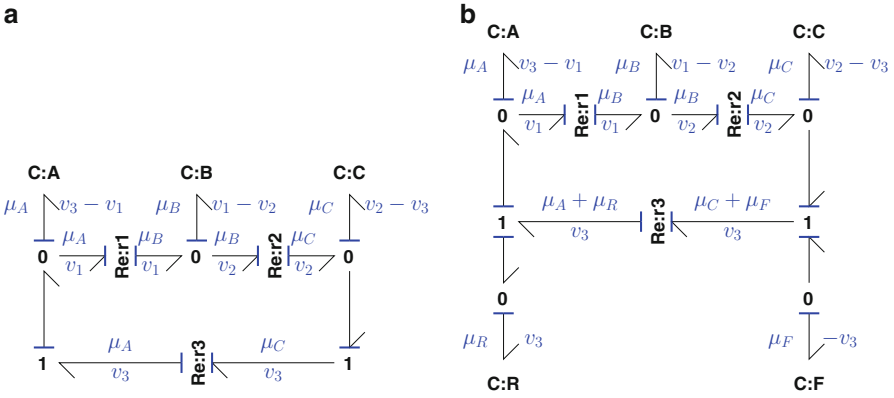

Fig. 16.2 Simple example. (**a**) $A \overset{1}{\rightleftharpoons} B \overset{2}{\rightleftharpoons} C \overset{3}{\rightleftharpoons} A$. The three **C** components represent the chemical species A, B and C respectively and the three **Re** components represent the corresponding reactions. These components are connected by bonds and **0** and **1** junctions which clearly show the cyclic nature of the reaction system. (**b**) Two additional species F and R are introduced and the third reaction of (**a**) is replaced by $C + F \overset{3}{\rightleftharpoons} A + R$. Causality has been completed with integral causality on the **C** components

Causality has been completed with integral causality on the **C** components using the sequential causality assignment procedure (SCAP) [21].[6]

The three **C** components correspond to the three species and are associated with states x_A, x_B and x_C and chemical potentials μ_A, μ_B and μ_C. The three reaction flows are v_1, v_2 and v_3 and are driven by the forward affinities $A_1^f = \mu_A$, $A_2^f = \mu_B$ and $A_3^f = \mu_C$ and by the reverse affinities $A_1^r = \mu_B$, $A_2^r = \mu_C$ and $A_3^r = \mu_A$. The state derivatives are

$$\dot{x}_A = v_3 - v_1 \tag{16.26}$$

$$\dot{x}_B = v_1 - v_2 \tag{16.27}$$

$$\dot{x}_C = v_2 - v_3 \tag{16.28}$$

and the chemical potentials are

$$\mu_A = RT \ln K_A x_A \tag{16.29}$$

$$\mu_B = RT \ln K_B x_B \tag{16.30}$$

$$\mu_C = RT \ln K_C x_C \tag{16.31}$$

[6]SCAP is used for all the examples in this chapter. Unless otherwise stated, all **C** components have integral causality.

and the reaction flows are

$$v_1 = \kappa_1 \left(e^{\frac{A_1^f}{RT}} - e^{\frac{A_1^r}{RT}} \right) = \kappa_1 \left(K_A x_A - K_B x_B \right) \tag{16.32}$$

$$v_2 = \kappa_2 \left(e^{\frac{A_2^f}{RT}} - e^{\frac{A_2^r}{RT}} \right) = \kappa_2 \left(K_B x_B - K_C x_C \right) \tag{16.33}$$

$$v_3 = \kappa_3 \left(e^{\frac{A_3^f}{RT}} - e^{\frac{A_3^r}{RT}} \right) = \kappa_3 \left(K_C x_C - K_A x_A \right) \tag{16.34}$$

These equations are *linear* because there is only one species on each side of each reaction.

Because of this linearity, the bond graph of Fig. 16.2a could have been represented using linear **C** components and replacing **Re** of Fig. 16.1a by the one port **R** and **1** junction version of Fig. 16.1b. Such an approach has two disadvantages: the resultant bond graph has no energy properties and would thus be a *pseudo bond graph* and such an approach is not scalable to more complex systems.

In particular, the extended system of Fig. 16.2b has the chemical equation of the third reaction replaced by

$$C + F \overset{3}{\rightleftharpoons} A + R \tag{16.35}$$

which has two species on each side of the reaction; and hence $A_3^f = \mu_C + \mu_f$ and $A_3^r = \mu_A + \mu_r$. Thus the reaction flow v_3 becomes

$$v_3 = \kappa_3 \left(e^{\frac{A_3^f}{RT}} - e^{\frac{A_3^r}{RT}} \right) = \kappa_3 \left(K_C K_F x_C x_F - K_A K_R x_A x_R \right) \tag{16.36}$$

This equation contains the product of states and is thus a *nonlinear* equation. This essential nonlinearity is a feature of biomolecular systems.

16.3 Structural Analysis

Although the properties of biomolecular systems arise from the non-linear behaviour of the **C** and **Re** components, the characteristics of each individual system depend on how these components are interconnected via the linear *junction structure* formed from bonds, **0** and **1** junctions.[7] Thus the analysis of such

[7] **TF** components representing reaction stoichiometry also occur—see example in Sect. 16.5.

junction structures reveals generic system properties which are independent of the parameters of the **C** and **Re** components.

Section 16.3.1 motivates the analysis using a hydraulic analogy of the simple biomolecular systems of Fig. 16.2. Section 16.3.2 looks at properties of *closed systems* where the junction structure transmits, but does not inject or consume energy. However, living systems are not *closed systems* but need to interact with the environment to replenish dissipated energy; hence Sect. 16.3.3 extends the analysis to *open systems* where such environmental interactions are modelled by *chemostats*. Section 16.3.4 shows how stoichiometric information can be deduced from the junction structure.

16.3.1 Motivation

Analogies are central to scientific thinking by providing a way for results and intuition form one physical domain to be transferred to another [24]. Bond graphs provide a formalism to discussing analogies. Thus, for example, the bond graph representing a network of biomolecular reactions has an electrical circuit representation [27]. Unfortunately, these circuits are quite complicated when more than one species is involved as substrate or product of a reaction—see Oster and Perelson [27, Fig. 6] for an example. However, for the purposes of motivation, the simple network of three reactions (16.25), modelled by the bond graph of Fig. 16.2a, is used as it does have simple analogies. Figure 16.3a gives an electrical circuit analogy and Fig. 16.3b gives a hydraulic analogy; the latter is used as a simple intuitive motivational example.

Consider the analogy of three open tanks of liquid Fig. 16.3b represented by the three **C** components connected by three narrow pipes represented by the three **Re**

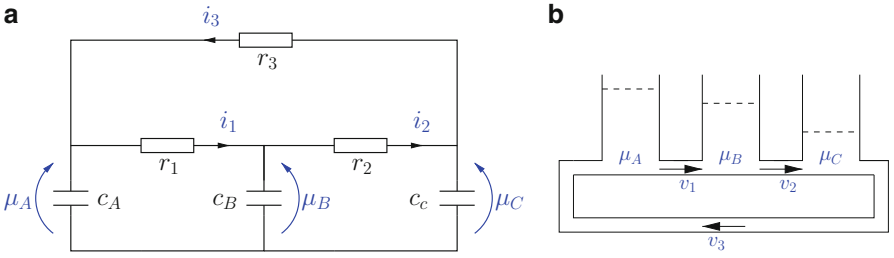

Fig. 16.3 Analogues of simple system. (**a**) An electric circuit analogue has three capacitors representing the three species and three resistors representing the three reactions; voltage is the analogue of chemical potential and current the analogue of molar flow rate. (**b**) A hydraulic analogy has three tanks of liquid representing the three species and three pipes representing the three reactions; pressure is the analogue of chemical potential and volumetric flow rate the analogue of molar flow rate. Linear analogies are only possible in simple cases such as this

components. μ_A, μ_B and μ_C then represent the pressures associated with the tanks and v_1, v_2 and v_3 the volumetric flow rates though the pipes.

In the linear case, the **C** components become linear and the **Re** components can be replaced by an **R** component and **1** junction as in Fig. 16.1 where in the case of **Re**:$\mathbf{r_1}$ the forward "affinity" or pressure $A_1^f = \mu_A$ and the reverse "affinity" or pressure $A_1^r = \mu_B$; the pressure drop across r_1 is $A_1 = A_1^f - A_1^r$. The following statements can be made about this particular system

1. The sum of the volumes of liquid in the three tanks (x_{tot}) is constant

$$x_A(t) + x_B(t) + x_C(t) = x_{\text{tot}} \tag{16.37}$$

   This is analogous to a *conserved moiety* in biochemistry.
2. As $A_1 + A_2 + A_3 = (\mu_A - \mu_B) + (\mu_B - \mu_C) + (\mu_C - \mu_A) = 0$, the sum of the three pressure drops is zero

$$A_1(t) + A_2(t) + A_3(t) = 0 \tag{16.38}$$

3. In the steady state of this closed system, there is no energy dissipation and so all flows are zero and thus the pressures are equal

$$\mu_A(\infty) = \mu_B(\infty) = \mu_C(\infty) \tag{16.39}$$

4. If the third pipe were replaced by a constant-flow pump with flow rate v_0, then in the steady state ($\dot{X} = 0$)

$$v_1(\infty) = v_2(\infty) = v_0 \tag{16.40}$$

These four statements are illustrated by the simulation of Fig. 16.4. Here all reaction constants and thermodynamics constants are unity ($\kappa_1 = \kappa_2 = \kappa_3 = K_A = K_B = K_C = 1$) and the initial states are $x_A = 3$, $x_B = 2.5$ and $x_C = 0.5$.

These four statements are obvious in the context of this simple system, the purpose of the next section is to show how these statements generalise to arbitrary biomolecular networks. The fourth statement involves the use of a pump. This requires an external source of energy and thus the resultant system is no longer closed. Thus the analysis is extended to include open as well as closed systems. The design of biomolecular pumps, and the source of their energy requirement, is key to understanding living systems. As will be discussed in Sect. 16.3.3, such pumps can be modelled using *chemostats* which are closely related to the bond graph effort source **Se**. Such pumps make use of the inherent non-linearity of biomolecular systems when multiple substrates and products of a reaction are present; in particular

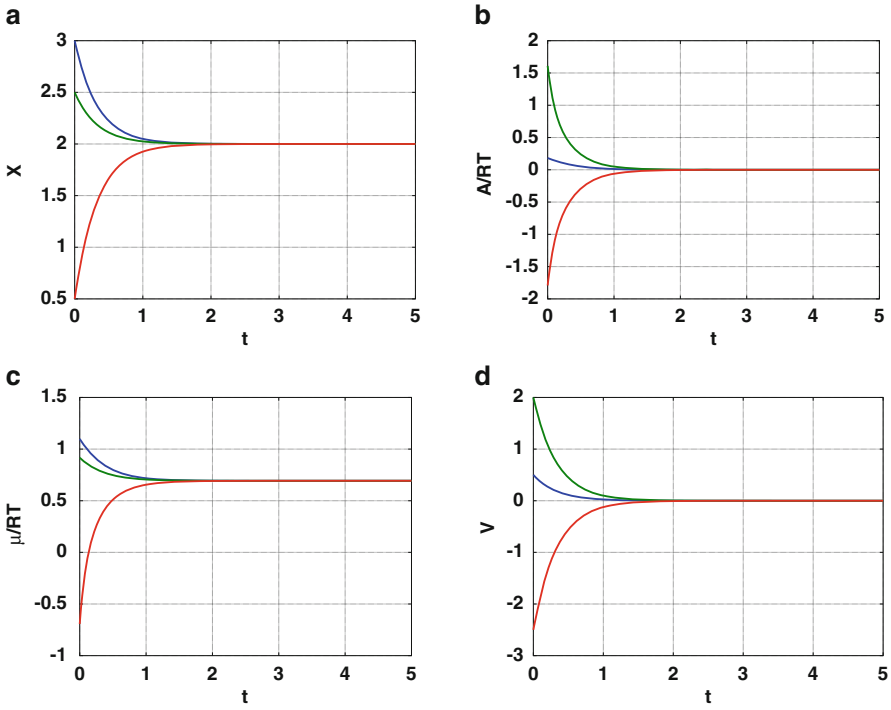

Fig. 16.4 Simulation of simple system. (**a**) The system states become constant in the steady state and their sum remains at the value 6 for all time: this corresponds to a *conserved moiety*. (**b**) The reaction affinities become zero in the steady state and their sum is 0 for all time. (**c**) The chemical potentials equalise in the steady state. (**d**) The reaction flows become zero in the steady state because this is a *closed* system

$ATP \rightleftharpoons ADP + P$[8] can be coupled multiplicatively to an underlying reaction to produce a pump; this is discussed further in Sect. 16.6.

16.3.2 Junction Structure of Closed Systems

This section is concerned with structural principles rather than details of component behaviour; hence, following Sect. 16.3.1, the **Re** component is replaced by a single-port **R** component and an associated **1** junction as in Fig. 16.1. The choice between

[8]*ATP* (Adenosine triphosphate) is the "fuel" which drives many biomolecular processes via its conversion to *ADP* (Adenosine diphosphate) and *P* inorganic phosphate [1].

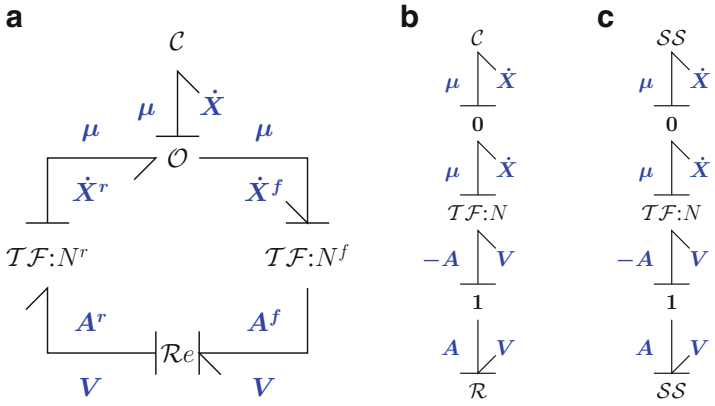

Fig. 16.5 General closed system with integral causality. (**a**) The general representation of a closed biomolecular system used by Gawthrop and Crampin [12]. (**b**) Simplified version with the two-port **Re** replaced by one-port **R** and **1** junction as in Fig. 16.1. (**c**) The **C** and **R** components are replaced by source-sensor (**SS**) components and *integral* causality is shown

the two representations is discussed by Karnopp [20]; in the context of this chapter, the **R** representation has the advantage that, via the **1** junction, it ensures continuity of flow.

The abstract representation of a closed system of Gawthrop et al. [13] and Gawthrop and Crampin [12] is given in Fig. 16.5a in terms of the **Re** reaction representation of Fig. 16.1a. The bond symbols $\rightharpoonup$ correspond to *vectors* of bonds; $\mathscr{C}, \mathscr{R}e$ and $\mathscr{O}$ correspond to arrays of **C**, **Re** and **0** components; the two $\mathscr{TF}$ components represent the intervening junction structure comprising bonds, **0** and **1** junctions and **TF** components. N^f and N^r are the forward and reverse stoichiometric matrices. Using the **R** reaction representation of Fig. 16.1b gives the simplified Fig. 16.5b where the stoichiometric matrix $N = N^r - N^f$.

The *multiport transformer* $\mathscr{TF}{:}N$ has the n_X vector $\boldsymbol{\mu}$ as the effort variable paired with the n_X vector $\dot{\boldsymbol{X}}$ as flow variable on one port and the n_V vector $-\boldsymbol{A}$ as the effort variable paired with the n_V vector $\boldsymbol{V}$ as flow variable on the other port. It follows that

$$\dot{\boldsymbol{X}} = N\boldsymbol{V} \tag{16.41}$$

$$\boldsymbol{A} = -N^T\boldsymbol{\mu} \tag{16.42}$$

This multiport transformer abstracts the connections between the n_X **C** components and the n_V **R** components; it is independent of the properties of the **C** and **R** components. It represents the junction structure of the underlying bond graph. In this paper, the junction structure is revealed by replacing each **C** and **R** component by

a *source-sensor* **SS** component [14, 15].[9] For example, the bond graph of Fig. 16.2a becomes the junction structure bond graph of Fig. 16.6a. The **SS** components have now preferred causality; in Fig. 16.6a the **SS** causality has been chosen to correspond to the preferred causality of Fig. 16.2a where the **C** components have integral causality (effort output) leading to flow output on each **R** component.

16.3.2.1 Structure Matrices

With the integral causality shown in Fig. 16.5c the junction structure *outputs* are the n_X **C** *flows* (rate of species change, $\dot{\boldsymbol{X}}$ mol s^{-1}) and the n_V **R** *efforts* (affinities, $\boldsymbol{A}$ J mol^{-1}). and the junction structure *inputs* are the n_X **C** *efforts* (chemical potentials, μ mol s^{-1}) and the n_V **R** *flows* (molar reaction flows, $\boldsymbol{V}$ mol s^{-1}). Combining the junction structure outputs into the vector $\boldsymbol{Y}$, and combining the junction structure inputs into the vector $\boldsymbol{U}$, Eqs. (16.41) and (16.42) can be rewritten in a more compact form as

$$\boldsymbol{Y} = S\boldsymbol{U} \tag{16.43}$$

$$\text{where } \boldsymbol{Y} = \begin{pmatrix} \dot{\boldsymbol{X}} \\ \boldsymbol{A} \end{pmatrix}, \ \boldsymbol{U} = \begin{pmatrix} \boldsymbol{\mu} \\ \boldsymbol{V} \end{pmatrix} \tag{16.44}$$

$$\text{and } S = \left(\begin{array}{c|c} 0_{n_X \times n_X} & N \\ \hline -N^T & 0_{n_V \times n_V} \end{array}\right) \tag{16.45}$$

The structure matrix S has two notable features:

1. As discussed, for example, by Karnopp et al. [21, Sect. 7.4] the *junction structure* matrix S is skew symmetric; this arises from the energy transmission properties of the multiport transformer.
2. The two block zero elements $0_{n_X \times n_X}$ and $0_{n_V \times n_V}$ arise because, in the junction structure, the effort and flow variables do not interact: biomolecular systems do *not* contain gyrators.

16.3.2.2 Derivative Causality

As was noted by Sueur and Dauphin-Tanguy [38, 39], investigating the junction structure with **C** and **I** components in *derivative causality* is the key to determining system properties. With this in mind, and noting that the only dynamic components are **C** components, the integral causality leading to S is replaced by maximising the

[9] The **SS** component is equivalent to the **EN** (environment) component introduced by Rosenberg and Andry [37].

number of **C** components in derivative causality. As noted by Sueur and Dauphin-Tanguy [39] with reference to their Fig. 2, the presence of causal loops requires a modification of this procedure; in particular, the causal loop must be broken by leaving a **C** component in integral causality.

This procedure will be referred to as *maximising derivative causality* in the sequel and leads to the concept of *derivative structure matrices*.

16.3.2.3 Derivative Structure Matrices

The vector $\boldsymbol{Y}_d$ contains the outputs of the network with maximum derivative causality and has four partitions:

1. $\boldsymbol{\mu}^D$ the chemical potential of the **SS** components corresponding to **C** in *derivative causality*.
2. $\dot{\boldsymbol{X}}^I$ the flow of the **SS** components corresponding to **C** remaining in *integral causality*.
3. $\boldsymbol{V}^D$ the flows of the **SS** components corresponding to **R** in *derivative causality*.
4. $\boldsymbol{A}^I$ the affinity of the **SS** components corresponding to **R** remaining in *integral causality*.

$\boldsymbol{Y}_d$ contains the same variables as $\boldsymbol{Y}$ but they may be in a different order. The vector $\boldsymbol{U}_d$ contains the covariables of $\boldsymbol{Y}_d$.

$\boldsymbol{Y}_d$ and $\boldsymbol{U}_d$ are related by the *derivative structure matrix* S_d where

$$\boldsymbol{Y}_d = S_d \boldsymbol{U}_d \tag{16.46}$$

$$\text{where } \boldsymbol{Y}_d = \begin{pmatrix} \boldsymbol{\mu}^D \\ \hline \dot{\boldsymbol{X}}^I \\ \hline \boldsymbol{V}^D \\ \hline \boldsymbol{A}^I \end{pmatrix}, \ \boldsymbol{U}_d = \begin{pmatrix} \dot{\boldsymbol{X}}^D \\ \hline \boldsymbol{\mu}^I \\ \hline \boldsymbol{A}^D \\ \hline \boldsymbol{V}^I \end{pmatrix} \tag{16.47}$$

$$\text{and } S_d = \left(\begin{array}{c|c|c|c} 0 & S_{\mu\mu} & S_{\mu A} & 0 \\ \hline S_{xx} & 0 & 0 & S_{xv} \\ \hline S_{vx} & 0 & 0 & S_{vv} \\ \hline 0 & S_{A\mu} & S_{AA} & 0 \end{array}\right) \tag{16.48}$$

As with S, S_d is skew symmetric because of energy considerations and the eight block zero elements arise as the effort and flow variables do not interact: biomolecular systems do *not* contain gyrators.

Example. In the case of the junction structure of Fig. 16.6a

$$N = \begin{pmatrix} -1 & 0 & 1 \\ 1 & -1 & 0 \\ 0 & 1 & -1 \end{pmatrix} \tag{16.49}$$

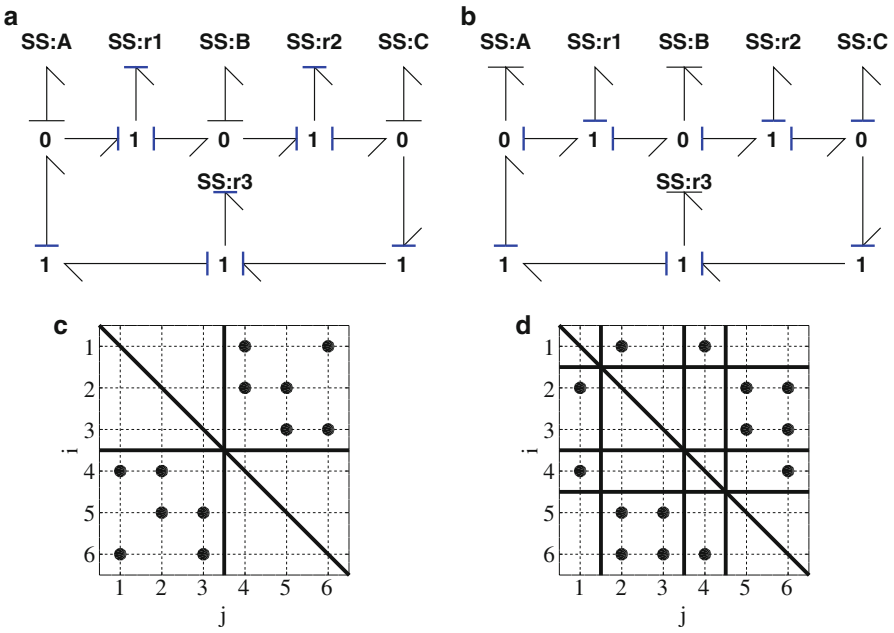

Fig. 16.6 Simple Closed System junction structure. (**a**) and (**b**) The junction structure corresponding to the bond graph of Fig. 16.2a with integral and maximum derivative causality respectively. (**c**) and (**d**) Alternative representation of the structure matrices S (16.43) and S_d (16.48) where *filled circle* indicates a non-zero entry and i and j the row and column indices respectively

and:

$$\boldsymbol{Y} = \begin{pmatrix} \dot{x}_A \\ \dot{x}_B \\ \dot{x}_C \\ \hline A_1 \\ A_2 \\ A_3 \end{pmatrix}, \; S = \left(\begin{array}{ccc|ccc} 0 & 0 & 0 & -1 & 0 & 1 \\ 0 & 0 & 0 & 1 & -1 & 0 \\ 0 & 0 & 0 & 0 & 1 & -1 \\ \hline 1 & -1 & 0 & 0 & 0 & 0 \\ 0 & 1 & -1 & 0 & 0 & 0 \\ -1 & 0 & 1 & 0 & 0 & 0 \end{array}\right), \; \boldsymbol{U} = \begin{pmatrix} \mu_A \\ \mu_B \\ \mu_C \\ \hline v_1 \\ v_2 \\ v_3 \end{pmatrix} \tag{16.50}$$

In the case of the junction structure of Fig. 16.6b with maximum derivative causality

$$\boldsymbol{Y}_d = \begin{pmatrix} \mu_A \\ \mu_B \\ \dot{x}_C \\ \hline v_1 \\ v_2 \\ A_3 \end{pmatrix}, \; S_d = \left(\begin{array}{cc|c|ccc} 0 & 0 & 1 & 1 & 1 & 0 \\ 0 & 0 & 1 & 0 & 1 & 0 \\ \hline -1 & -1 & 0 & 0 & 0 & 0 \\ \hline -1 & 0 & 0 & 0 & 0 & 1 \\ -1 & -1 & 0 & 0 & 0 & 1 \\ \hline 0 & 0 & 0 & -1 & -1 & 0 \end{array}\right), \; \boldsymbol{U}_d = \begin{pmatrix} \dot{x}_A \\ \dot{x}_B \\ \mu_C \\ \hline A_1 \\ A_2 \\ v_3 \end{pmatrix} \tag{16.51}$$

As an alternative to Eqs. (16.50) and (16.51), the structure matrices S and S_d can be visualised by the diagrams of Fig. 16.6c, d where the ij non-zero matrix elements are plotted as • in the ij location. The partition lines separating $\dot{\boldsymbol{X}}$ from $\boldsymbol{A}$ and $\boldsymbol{\mu}$ from $\boldsymbol{V}$ have been included for clarity along with the diagonal about which the matrix is skew symmetric. This representation is particularly useful for large systems when the matrix expression becomes unwieldy.

The four observations of Sect. 16.3.1 can now be explained in terms of the partitions of the S_d matrix (16.48) and (16.51).

1. From the second row partition

$$S_{xx} = \begin{pmatrix} -1 & -1 \end{pmatrix} \tag{16.52}$$

$$\text{hence } \dot{x}_C = -\dot{x}_A - \dot{x}_B \tag{16.53}$$

$$\text{and } \dot{x}_A + \dot{x}_B + \dot{x}_C = 0 \tag{16.54}$$

   Integrating (16.54) with respect to time gives Eq. (16.37).
2. From the fourth row partition

$$S_{AA} = \begin{pmatrix} -1 & -1 \end{pmatrix} \tag{16.55}$$

$$\text{hence } A_3 = -A_1 - A_2 \tag{16.56}$$

   Rearranging Eq. (16.56) gives Eq. (16.38).
3. From the first row partition

$$S_{\mu\mu} = \begin{pmatrix} 1 \\ 1 \end{pmatrix}, \; S_{\mu A} = \begin{pmatrix} 1 & 1 \\ 0 & 1 \end{pmatrix} \tag{16.57}$$

$$\text{hence } \mu_A = A_1 + A_2 + \mu_C \tag{16.58}$$

$$\mu_B = A_2 + \mu_C \tag{16.59}$$

   In the steady state, the flows are zero $v_1 = v_2 = v_3 = 0$ and thus the affinities are also zero $A_1 = A_2 = A_3 = 0$; substituting into Eqs. (16.58) and (16.59) gives Eq. (16.39).
4. From the third row partition

$$S_{vv} = \begin{pmatrix} 1 \\ 1 \end{pmatrix}, \; S_{vx} = \begin{pmatrix} -1 & 0 \\ -1 & -1 \end{pmatrix} \tag{16.60}$$

$$\text{hence } v_1 = -\dot{x}_A + v_3 \tag{16.61}$$

$$v_2 = -\dot{x}_A - \dot{x}_B + v_3 \tag{16.62}$$

Setting $\dot{x}_A = \dot{x}_B = 0$ gives Eq. (16.40). Of course, in this closed system, the three steady-state flows are actually zero; to obtain "pumping" and non-zero flows we now turn to consideration of *open* systems.

16.3.3 Junction Structure of Open Systems

All living systems are connected to their environment: mass and energy can enter and leave the system. Thus living systems are *open* systems and, for this reason, this section considers the junction structures of open systems. Following Gawthrop and Crampin [12], thermodynamically closed systems are converted to thermodynamically open systems using *chemostats*.[10]

Gawthrop and Crampin [12] also use *flowstats*.[11] But this idea is not pursued in this chapter.

As discussed by Gawthrop and Crampin [12], a chemostat generates a chemical potential μ which is not dependent on the flow covariable $\dot{x}$ and may be modelled as a **C** component with a fixed state. For the purposes of junction structure analysis it is convenient to represent the chemostat by a **C** component and a unit *effort amplifier* **AE** [15] component where the **AE** component has unit gain and infinite input impedance thus drawing zero flow from the **C** component; see Fig. 16.7a. The **AE** component has fixed causality as indicated in Fig. 16.7b; the input and output of the **AE** are explicitly indicated to avoid ambiguity. The **AE** component is *active* and thus represents the power source of an open system.

As in Sect. 16.3.2, the junction structure is obtained from the system bond graph by replacing each **C** and **R** component by a *source-sensor* **SS** component; this leaves the **AE** components associated with chemostats as part of the junction structure. This has a number of consequences:

1. The junction structure is no longer energy conserving; the chemostats insert energy into the system.
2. Equations (16.41) and (16.42) are replaced by:

$$\dot{\boldsymbol{X}} = N^{cd}\boldsymbol{V} \tag{16.63}$$

$$\boldsymbol{A} = -N^T\boldsymbol{\mu} \tag{16.64}$$

[10] The term *chemostat* was used by Polettini and Esposito [35] and is equivalent to the "concentration clamping" of Qian and Beard [36].

[11] The term *flowstat* is equivalent to "boundary flux injection" [36].

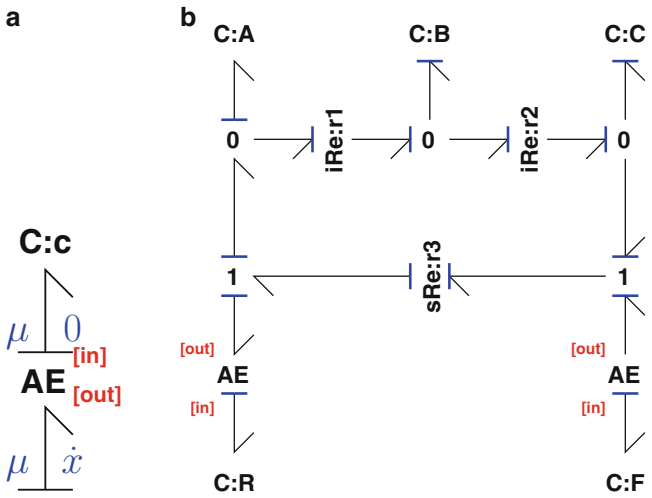

Fig. 16.7 Chemostats. (**a**) A *chemostat* is modelled by a **C** component and a **AE** effort amplifier; this means that the corresponding chemical potential μ is imposed on the rest of the system but the corresponding flow $\dot{x}$ does not effect the **C** component. (**b**) The simple example of Fig. 16.2b is modified with **AE** components to turn **C**:**F** and **C**:**R** into chemostats thus creating an open system from a closed system

where N^{cd} is N with rows corresponding to the chemostats removed [12, Sect. 3.4]. The structure matrix S is no longer of the skew symmetric form of Eq. (16.45) but is rather of the form

$$S = \left(\begin{array}{c|c} 0 & N^{cd} \\ \hline -N^T & 0 \end{array}\right) \tag{16.65}$$

3. When maximising derivative causality, the possible causal patterns of the junction structure are constrained by the fixed causality of the **AE** components.

16.3.3.1 Example (Chemostats)

The closed system of Fig. 16.6 is turned into the open system of Fig. 16.7b where the flow v_3 is "pumped" by the addition of a forward-driving chemostat **C**:**F** and a reverse-driving chemostat **C**:**R** arranged so that there is no net mass inflow to the system. This is the chemostatic version of the chemical equation (16.35) with the bond graph of Fig. 16.2b. Figure 16.8a shows the corresponding junction structure in integral causality and Fig. 16.8b with maximum derivative causality.

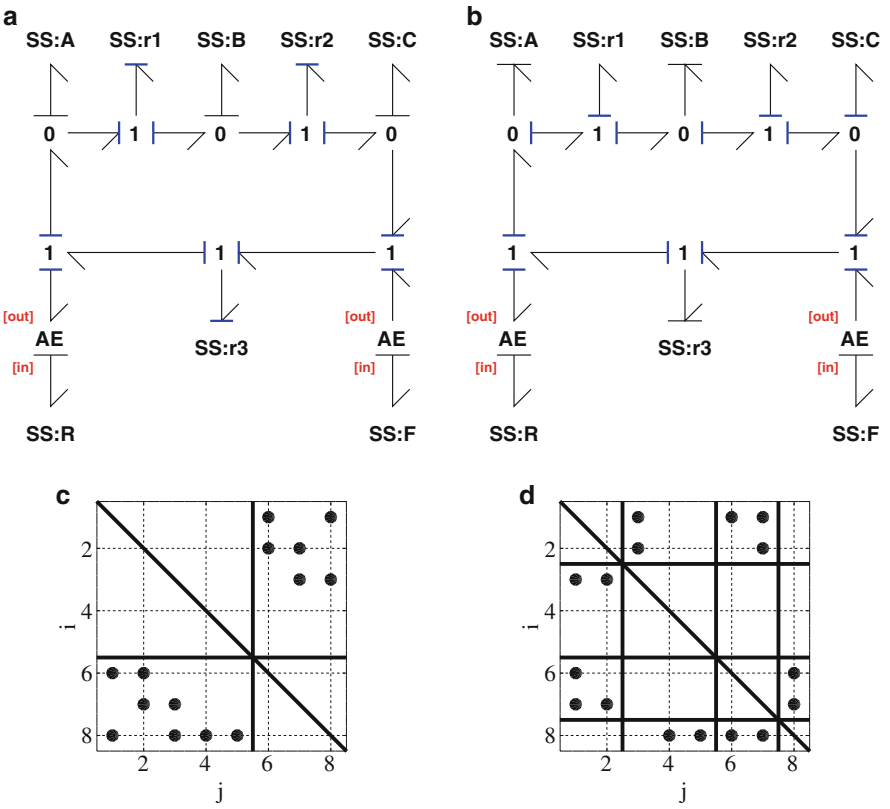

Fig. 16.8 Simple open system junction structure. (**a**) and (**b**) The junction structure corresponding to the bond graph of Fig. 16.7b with integral and maximum derivative causality respectively. (**c**) and (**d**) Alternative representation of the structure matrices S (16.43) and S_d (16.48) where *filled circle* indicates a non-zero entry and i and j the row and column indices respectively. Note that these matrices are no longer skew-symmetric due to the **AE** components and that the driving term $S_{A\mu}$ is no longer zero

The corresponding structure matrix S is

$$\boldsymbol{Y} = \begin{pmatrix} \dot{x}_A \\ \dot{x}_B \\ \dot{x}_C \\ \dot{x}_F \\ \dot{x}_R \\ \hline A_1 \\ A_2 \\ A_3 \end{pmatrix}, \; S = \left(\begin{array}{ccccc|ccc} 0 & 0 & 0 & 0 & 0 & -1 & 0 & 1 \\ 0 & 0 & 0 & 0 & 0 & 1 & -1 & 0 \\ 0 & 0 & 0 & 0 & 0 & 0 & 1 & -1 \\ 0 & 0 & 0 & 0 & 0 & 0 & 0 & 0 \\ 0 & 0 & 0 & 0 & 0 & 0 & 0 & 0 \\ \hline 1 & -1 & 0 & 0 & 0 & 0 & 0 & 0 \\ 0 & 1 & -1 & 0 & 0 & 0 & 0 & 0 \\ -1 & 0 & 1 & 1 & -1 & 0 & 0 & 0 \end{array}\right), \; \boldsymbol{U} = \begin{pmatrix} \mu_A \\ \mu_B \\ \mu_C \\ \mu_F \\ \mu_R \\ \hline v_1 \\ v_2 \\ v_3 \end{pmatrix} \tag{16.66}$$

The corresponding derivative-causality structure matrix S_d is

$$\boldsymbol{Y}_d = \begin{pmatrix} \mu_A \\ \mu_B \\ \hline \dot{x}_C \\ \dot{x}_F \\ \dot{x}_R \\ \hline v_1 \\ v_2 \\ \hline A_3 \end{pmatrix}, \; S_d = \left(\begin{array}{cc|ccc|cc|c} 0 & 0 & 1 & 0 & 0 & 1 & 1 & 0 \\ 0 & 0 & 1 & 0 & 0 & 0 & 1 & 0 \\ \hline -1 & -1 & 0 & 0 & 0 & 0 & 0 & 0 \\ 0 & 0 & 0 & 0 & 0 & 0 & 0 & 0 \\ 0 & 0 & 0 & 0 & 0 & 0 & 0 & 0 \\ \hline -1 & 0 & 0 & 0 & 0 & 0 & 0 & 1 \\ -1 & -1 & 0 & 0 & 0 & 0 & 0 & 1 \\ \hline 0 & 0 & 0 & 1 & -1 & -1 & -1 & 0 \end{array}\right), \; \boldsymbol{U}_d = \begin{pmatrix} \dot{x}_A \\ \dot{x}_B \\ \hline \mu_C \\ \mu_F \\ \mu_R \\ \hline A_1 \\ A_2 \\ \hline v_3 \end{pmatrix} \tag{16.67}$$

Again, S (16.66) and S_d (16.67) can be visualised using Fig. 16.8c, d.

S_d for the open system (16.67) differs from that from the closed system (16.51) in a number of ways.

1. The fourth row partition contains the driving term $\mu_f - \mu_r$ in the second column partition.
2. The two zero rows in the second row partition correspond to the two chemostats; in addition to the conserved moiety of Eq. (16.37), the two chemostats correspond to the two conserved moieties x_F and x_R.

Figure 16.9 gives a simulation of the simple system with chemostatic pump. Like the simulation shown in Fig. 16.4, all quantities tend to constant values; but, unlike the simulation shown in Fig. 16.4, the flows (v) and affinities (A) tend to non-zero constant values: the two chemostats **C**:**F** and **C**:**R** act as a pump.

16.3.4 Stoichiometric Information and Simulation

The *stoichiometric matrix* N of a biomolecular network is the matrix that relates the reaction flows described by the vector $\boldsymbol{V}$ to the rate of change of species described by the vector $\dot{\boldsymbol{X}}$ as in Eq. (16.41). As discussed in the text books of Palsson [30], Alon [2] and Klipp et al. [22], analysis of the stoichiometric matrix yields useful information about the properties of the underlying biomolecular network. In particular the *null space* or *kernel* space of both N and N^T are of interest and are defined by the corresponding kernel, or subspace, matrices. The null space of N relates to those linear combinations of reaction flows which can be non-zero when $\dot{\boldsymbol{X}}$ is zero; the null space of N^T relates to *conserved moieties*: those linear combinations of $\boldsymbol{X}$ which remain constant.

The structure matrix S_d (16.48), corresponding to maximum derivative causality, contains eight non-zero submatrices. This section provides interpretations of these matrices and how they relate to the kernel matrices of the stoichiometric matrix.

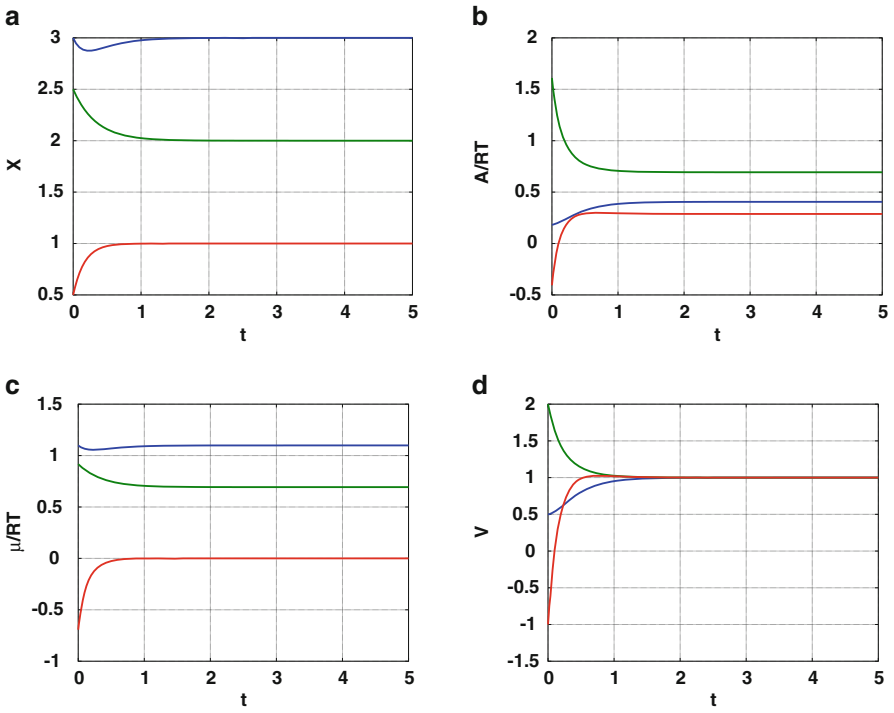

Fig. 16.9 Simulation of simple system with chemostatic pump. $K_F = K_R = 1$, $x_F = 4$ and $x_R = 1$ (**a**) As in the closed case, the system states become constant in the steady state and their is sum 6 for all time. (**b**) The reaction affinities become constant in the steady state and their sum is $\ln K_F x_F - \ln K_R x_R = 1.386$ for all time. (**c**) The chemical potentials no longer equalise in the steady state. (**d**) The reaction flows are not zero in the steady state as this is an open system with F and R acting as a pump

16.3.4.1 State Reconstruction

The vectors Y_d and U_d (16.47) partition the state vector derivative $\dot{\boldsymbol{X}}$ into $\dot{\boldsymbol{X}}^I$ and $\dot{\boldsymbol{X}}^D$ and the flow vector $\boldsymbol{V}$ into $\boldsymbol{V}^I$ and $\boldsymbol{V}^D$. This decomposition process can be written as

$$\dot{\boldsymbol{X}}^I = T_{xi}\dot{\boldsymbol{X}},\ \dot{\boldsymbol{X}}^D = T_{xd}\dot{\boldsymbol{X}} \tag{16.68}$$

$$\boldsymbol{V}^I = T_{vi}\boldsymbol{V},\ \boldsymbol{V}^D = T_{vd}\boldsymbol{V} \tag{16.69}$$

Equations (16.68) and (16.69) can be rewritten as:

$$\begin{pmatrix} \dot{\boldsymbol{X}}^I \\ \dot{\boldsymbol{X}}^d \end{pmatrix} = T_x\dot{\boldsymbol{X}} \text{ where } T_x = \begin{pmatrix} T_{xi} \\ T_{xd} \end{pmatrix} \tag{16.70}$$

$$\text{and } \begin{pmatrix} \boldsymbol{V}^I \\ \boldsymbol{V}^d \end{pmatrix} = T_v \boldsymbol{V} \text{ where } T_v = \begin{pmatrix} T_{vi} \\ T_{vd} \end{pmatrix} \tag{16.71}$$

Because T_x and T_v permute the elements of $\dot{\boldsymbol{X}}$ and $\boldsymbol{V}$, they are unitary matrices and therefore

$$T_x^{-1} = T_x^T = \left(T_{xi}^T \middle| T_{xd}^T \right) \tag{16.72}$$

$$\text{and } T_v^{-1} = T_v^T = \left(T_{vi}^T \middle| T_{vd}^T \right) \tag{16.73}$$

It follows that $\dot{\boldsymbol{X}}$ and $\boldsymbol{V}$ can be recomposed as

$$\dot{\boldsymbol{X}} = T_{xi}^T \dot{\boldsymbol{X}}^I + T_{xd}^T \dot{\boldsymbol{X}}^D \tag{16.74}$$

$$\boldsymbol{V} = T_{vi}^T \boldsymbol{V}^I + T_{vd}^T \boldsymbol{V}^D \tag{16.75}$$

Using (16.74) and the second partition of structure matrix S_d (16.48), $\dot{\boldsymbol{X}}$ can be expressed in terms of $\dot{\boldsymbol{X}}^D$ as

$$\begin{aligned} \dot{\boldsymbol{X}} &= T_{xi}^T \left(S_{xx} \dot{\boldsymbol{X}}^D + S_{xv} V^I \right) + T_{xd}^T \dot{\boldsymbol{X}}^D \\ &= L_{Xx} \dot{\boldsymbol{x}} + L_{Xv} V^I \end{aligned} \tag{16.76}$$

$$\text{where } \dot{\boldsymbol{x}} = \dot{\boldsymbol{X}}^D,\ L_{Xx} = \left(T_{xi}^T S_{xx} + T_{xd}^T \right),\ L_{Xv} = T_{xi}^T S_{xv} \tag{16.77}$$

When $L_{Xv} = 0$ (as in all the examples in this chapter)

$$\dot{\boldsymbol{X}} = L_{Xx} \dot{\boldsymbol{x}} \tag{16.78}$$

Integrating with respect to time gives

$$\boldsymbol{X} = L_{Xx} \boldsymbol{x} + G_X \boldsymbol{X}_0 \tag{16.79}$$

$$\text{where } G_X = I_{n_X \times n_X} - L_{Xx} T_{xd} \tag{16.80}$$

$$\text{and } \boldsymbol{X}_0 = \boldsymbol{X}(0) \tag{16.81}$$

As discussed by Gawthrop and Crampin [11, Sect. 4(c)], Eq. (16.79) is useful because it allows the system ODE to be solved for $\boldsymbol{x}$ which is of lower dimension than $\boldsymbol{X}$ and avoids issues with conserved moieties. For compatibility with previous work, and with reference to Eq. (16.68), it is convenient to define

$$L_{xX} = T_{xd} \tag{16.82}$$

$$\text{so that } \boldsymbol{x} = L_{xX} \boldsymbol{X} \tag{16.83}$$

16.3.4.2 Kernel Matrices

In the particular case that $S_{xv} = 0$, it follows from Eq. (16.47) and the second row partition of (16.48) that

$$\dot{\boldsymbol{X}}^I - S_{xx}\dot{\boldsymbol{X}}^D = 0 \tag{16.84}$$

Using the decomposition equations (16.68), (16.84) gives

$$G^{cd}\dot{\boldsymbol{X}} = 0 \tag{16.85}$$

$$\text{where } G^{cd} = T_{xi} - S_{xx}T_{xd} \tag{16.86}$$

Using Eq. (16.63), it follows from Eq. (16.85) that:

$$G^{cd}N^{cd}\boldsymbol{V} = 0 \tag{16.87}$$

As Eq. (16.87) must be true for all $\boldsymbol{V}$, it follows that

$$G^{cd}N^{cd} = 0 \tag{16.88}$$

Hence G^{cd} is the left kernel matrix of N^{cd}.

In the steady state, $\dot{\boldsymbol{X}}^D = 0$ and so, using the third row partition of (16.48)

$$\boldsymbol{V}^D = S_{vv}\boldsymbol{V}^I \tag{16.89}$$

hence, using the recomposition equation (16.75):

$$\boldsymbol{V} = K^{cd}\boldsymbol{V}^I \tag{16.90}$$

$$\text{where } K^{cd} = T_{vi}^T + T_{vd}^T S_{vv} \tag{16.91}$$

Using Eq. (16.90), the steady-state condition also implies that

$$\dot{\boldsymbol{X}} = N^{cd}\boldsymbol{V} = N^{cd}K^{cd}\boldsymbol{V}^I = 0 \tag{16.92}$$

As this must be true for all $\boldsymbol{V}^I$ it follows that

$$N^{cd}K^{cd} = 0 \tag{16.93}$$

and thus K^{cd} is the right kernel matrix of N^{cd}.

Kernel matrices can be found numerically from N^{cd} using Gaussian elimination. However, the approach here gives a clear physical derivation of the kernel matrices using causality arguments.

Example. The open system of Sect. 16.3.3 with the junction structure of Fig. 16.8 has structure matrices S and S_d given by Eqs. (16.66) and (16.67). In this case

$$T_{xi} = \begin{pmatrix} 0&0&1&0&0 \\ 0&0&0&1&0 \\ 0&0&0&0&1 \end{pmatrix}, \; T_{xd} = \begin{pmatrix} 1&0&0&0&0 \\ 0&1&0&0&0 \end{pmatrix}, \; L_{xX} = \begin{pmatrix} 1&0&0&0&0 \\ 0&1&0&0&0 \end{pmatrix} \tag{16.94}$$

$$L_{Xx} = \begin{pmatrix} 1&0 \\ 0&1 \\ -1&-1 \\ 0&0 \\ 0&0 \end{pmatrix}, \; G_X = \begin{pmatrix} 0&0&0&0&0 \\ 0&0&0&0&0 \\ 1&1&1&0&0 \\ 0&0&0&1&0 \\ 0&0&0&0&1 \end{pmatrix} \tag{16.95}$$

L_{xX} (16.94) reflects the fact that $\boldsymbol{x}$ contains the first two states x_A and x_B of $\boldsymbol{X}$ and L_{xX} (16.95) reflects the fact that the third state x_C is related to the first two via a conserved moiety as does the third row of G_X (16.95). The last two rows of G_X (16.95) correspond to the constant states of the two chemostats.

The two kernel matrices are

$$G^{cd} = \begin{pmatrix} 1&1&1&0&0 \\ 0&0&0&1&0 \\ 0&0&0&0&1 \end{pmatrix} \tag{16.96}$$

$$K^{cd} = \begin{pmatrix} 1 \\ 1 \\ 1 \end{pmatrix} \tag{16.97}$$

The first row of G^{cd} (16.96) again reflects the conserved moiety and the last two rows correspond to the two chemostats. The single column of K^{cd} (16.97) corresponds to the pathway though the three reaction components.

16.4 Example: Biomolecular Cycle

In his classic monograph, "Free energy transduction and biochemical cycle kinetics" Hill [17] discusses how the concentration difference of a species M existing both outside (M_o) and inside (M_i) a membrane can be used to pump another species L from inside (L_i) to outside (L_o) the membrane. This cycle uses a large protein molecule with two con formations E and E^*[12] the former allowing successive

[12] A protein molecule with a given chemical composition may have many different geometric "shapes" or conformations with different Gibbs energy—this is the basis of much cell biology [1].

binding to M_i and L_i and the latter to M_o and L_o. This is represented by seven reactions

$$M_i + E \overset{em}{\rightleftharpoons} EM \tag{16.98}$$

$$L_i + EM \overset{lem}{\rightleftharpoons} LEM \tag{16.99}$$

$$LEM \overset{lesm}{\rightleftharpoons} LE^\star M \tag{16.100}$$

$$LE^\star M \overset{esm}{\rightleftharpoons} L_o + E^\star M \tag{16.101}$$

$$E^\star M \overset{es}{\rightleftharpoons} M_o + E^\star \tag{16.102}$$

$$E^\star \overset{e}{\rightleftharpoons} E \tag{16.103}$$

$$EM \overset{\text{slip}}{\rightleftharpoons} E^\star M \tag{16.104}$$

where the last reaction is the so-called slip term. The corresponding bond graph appears in Fig. 16.10a where $E^\star$ is replaced by Es. The bond graph clearly shows the cyclic structure of the chemical reactions (16.98)–(16.104) and is topologically similar to the diagram of Hill [17, Fig. 1.2(a)]. As discussed by Hill [17], the four species M_o, M_i, L_o and L_i are assumed to have constant concentration: therefore they are modelled by four chemostats with the corresponding **AE** components.

The partitions of $\boldsymbol{Y}$ corresponding to Eq. (16.43) are

$$\dot{\boldsymbol{X}} = \begin{pmatrix} \dot{x}_{EM} & \dot{x}_{LEM} & \dot{x}_{Es} & \dot{x}_{EsM} & \dot{x}_{LEsM} & \dot{x}_{Li} & \dot{x}_{Lo} & \dot{x}_{Mi} & \dot{x}_{Mo} & \dot{x}_E \end{pmatrix}^T \tag{16.105}$$

$$\boldsymbol{A} = \begin{pmatrix} A_{em} & A_{lem} & A_{es} & A_{esm} & A_{\text{slip}} & A_e & A_{lesm} \end{pmatrix}^T \tag{16.106}$$

and the partitions of $\boldsymbol{U}$ corresponding to Eq. (16.43) are

$$\boldsymbol{\mu} = \begin{pmatrix} \mu_{EM} & \mu_{LEM} & \mu_{Es} & \mu_{EsM} & \mu_{LEsM} & \mu_{Li} & \mu_{Lo} & \mu_{Mi} & \mu_{Mo} & \mu_E \end{pmatrix}^T \tag{16.107}$$

$$\boldsymbol{V} = \begin{pmatrix} v_{em} & v_{lem} & v_{es} & v_{esm} & v_{\text{slip}} & v_e & v_{lesm} \end{pmatrix}^T \tag{16.108}$$

The partitions of $\boldsymbol{Y}_d$ corresponding to Eq. (16.47) are

$$\boldsymbol{\mu}^D = \begin{pmatrix} \mu_{EM} & \mu_{LEM} & \mu_{Es} & \mu_{EsM} & \mu_{LEsM} \end{pmatrix}^T \tag{16.109}$$

$$\dot{\boldsymbol{X}}^I = \begin{pmatrix} \dot{x}_{Li} & \dot{x}_{Lo} & \dot{x}_{Mi} & \dot{x}_{Mo} & \dot{x}_E \end{pmatrix}^T \tag{16.110}$$

$$\boldsymbol{V}^D = \begin{pmatrix} v_{em} & v_{lem} & v_{es} & v_{esm} & v_{\text{slip}} \end{pmatrix}^T \tag{16.111}$$

$$\boldsymbol{A}^I = \begin{pmatrix} A_e & A_{lesm} \end{pmatrix}^T \tag{16.112}$$

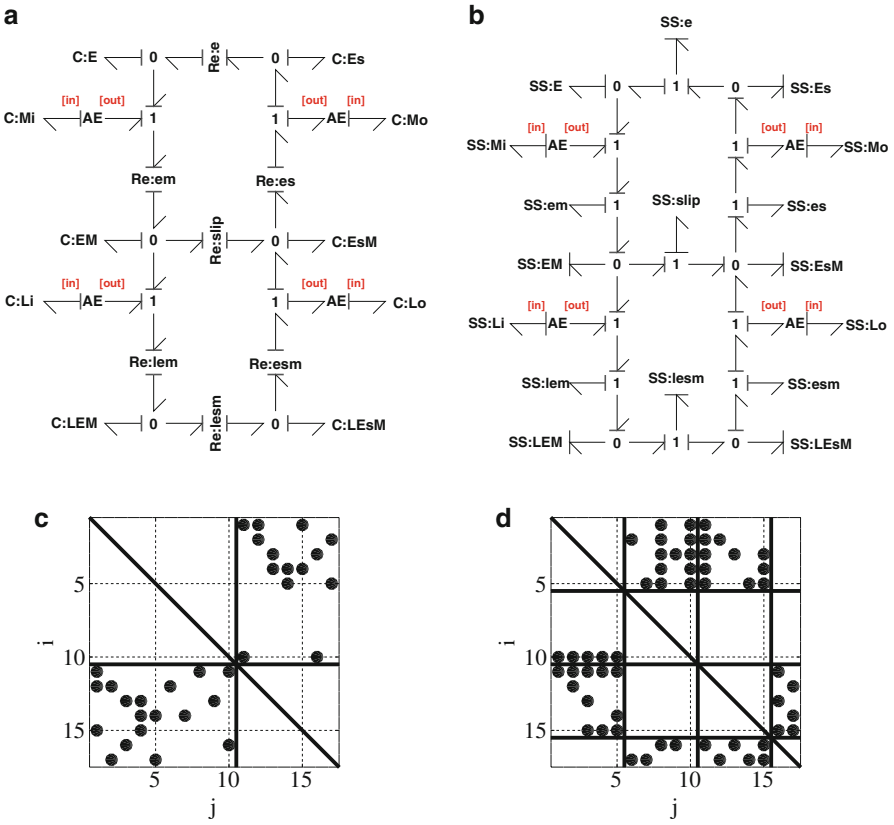

Fig. 16.10 Biomolecular Cycle. This example is taken from Hill [17] and shows how one species can pump another across a membrane. (**a**) System bond graph. (**b**) Junction structure with maximum derivative causality. (**c**) and (**d**) Alternative representation of the structure matrices S (16.43) and S_d (16.48) where *filled circle* indicates a non-zero entry and i and j the row and column indices respectively

and the partitions of $\boldsymbol{U}_d$ corresponding to Eq. (16.47) are

$$\dot{\boldsymbol{X}}^D = \left(\dot{x}_{EM}\ \dot{x}_{LEM}\ \dot{x}_{Es}\ \dot{x}_{EsM}\ \dot{x}_{LEsM}\right)^T \tag{16.113}$$

$$\boldsymbol{\mu}^I = \left(\mu_{Li}\ \mu_{Lo}\ \mu_{Mi}\ \mu_{Mo}\ \mu_E\right)^T \tag{16.114}$$

$$\boldsymbol{A}^D = \left(A_{em}\ A_{lem}\ A_{es}\ A_{esm}\ A_{\text{slip}}\right)^T \tag{16.115}$$

$$\boldsymbol{V}^I = \left(v_e\ v_{lesm}\right)^T \tag{16.116}$$

The 17×17 matrix S_d is summarised in Fig. 16.10d. The relevance of the submatrices S_{xx}, S_{AA}, $S_{A\mu}$ and S_{vv} are now examined in turn.

1. From the second row partition

$$S_{xx} = \begin{pmatrix} 0 & 0 & 0 & 0 & 0 \\ 0 & 0 & 0 & 0 & 0 \\ 0 & 0 & 0 & 0 & 0 \\ 0 & 0 & 0 & 0 & 0 \\ -1 & -1 & -1 & -1 & -1 \end{pmatrix} \tag{16.117}$$

the first four rows of S_{xx} correspond to the four chemostats *Li*, *Lo*, *Mi* and *Mo*.

$$\dot{x}_{Li} = \dot{x}_{Lo} = \dot{x}_{Mi} = \dot{x}_{Mo} = 0 \tag{16.118}$$

The fifth row of S_{xx} corresponds to the conserved moiety

$$\dot{x}_e + \dot{x}_{em} + \dot{x}_{lem} + \dot{x}_{es} + \dot{x}_{esm} + \dot{x}_{lesm} = 0 \tag{16.119}$$

2. From the fourth row partition

$$S_{AA} = \begin{pmatrix} -1 & 0 & -1 & 0 & -1 \\ 0 & -1 & 0 & -1 & 1 \end{pmatrix} \text{ and } S_{A\mu} = \begin{pmatrix} 0 & 0 & 1 & -1 & 0 \\ 1 & -1 & 0 & 0 & 0 \end{pmatrix} \tag{16.120}$$

the first row of S_{AA}, together with the first row of $S_{A\mu}$, corresponds to the sum of the affinities around the upper loop of the biomolecular cycle of Fig. 16.10a being equal to the weighted sum of the relevant chemostat potentials

$$A_e + A_{em} + A_{es} + A_{\text{slip}} = \mu_{Mi} - \mu_{Mo} \tag{16.121}$$

the second row of S_{AA}, together with the second row of $S_{A\mu}$, corresponds to the weighted sum of the affinities around the lower loop of the biomolecular cycle of Fig. 16.10a being equal to the weighted sum of the relevant chemostat potentials

$$A_{lesm} + A_{lem} + A_{esm} - A_{\text{slip}} = \mu_{li} - \mu_{lo} \tag{16.122}$$

3. From the third row partition

$$S_{vv} = \begin{pmatrix} 1 & 0 \\ 0 & 1 \\ 1 & 0 \\ 0 & 1 \\ 1 & -1 \end{pmatrix} \tag{16.123}$$

In the steady state ($\dot{\boldsymbol{X}} = 0$). In this case the first four rows of the first column of S_{vv} correspond to the three steady-state reaction flows in the upper loop being equal

$$v_{em} = v_{es} = v_e \tag{16.124}$$

Similarly, the first four rows of the second column of S_{vv} correspond to the three steady-state reaction flows in the lower loop being equal

$$v_{lem} = v_{esm} = v_{lesm} \tag{16.125}$$

and the fifth row of S_{vv} corresponds to the slip flow being the difference of the two loop flows

$$v_{\text{slip}} = v_e - v_{lesm} \tag{16.126}$$

16.5 Example: Glycolysis

Metabolism converts energy from the environment into the fuel that drives living processes. One example of metabolism is *glycolysis* which converts the chemical energy stored in glucose to the chemical energy stored in ATP (which, as discussed in Footnote 8, fuels biomolecular systems) and NADH.[13] Detailed mathematical models of glycolysis are given by Lambeth and Kushmerick [23] and Beard [4].

As bond graphs focus on energy transduction, it follows that bond graphs provide a natural method to model metabolism. Gawthrop et al. [13] develop a hierarchical bond graph model of metabolism based on that of Lambeth and Kushmerick [23] and highlight the advantages of the bond graph approach. This example looks at a simplified model of glycolysis used by Cloutier et al. [8] in the context of metabolism in the human brain and illustrates the junction structure approach to analysing the key properties of glycolysis.

The partitions of Y are

$$\dot{\boldsymbol{X}} = \left(\dot{x}_{G6P}\ \dot{x}_{F6P}\ \dot{x}_{GAP}\ \dot{x}_{PEP}\ \dot{x}_{ATP}\ \dot{x}_{ADP}\ \dot{x}_{NAD}\ \dot{x}_{NADH}\ \dot{x}_{GLC}\ \dot{x}_{PYR}\right)^T \tag{16.127}$$

$$\boldsymbol{A} = \left(A_{PGI}\ A_{PFK}\ A_{PGK}\ A_{PK}\ A_{HK}\right)^T \tag{16.128}$$

and the partitions of U are

$$\boldsymbol{\mu} = \left(\mu_{G6P}\ \mu_{F6P}\ \mu_{GAP}\ \mu_{PEP}\ \mu_{ATP}\ \mu_{ADP}\ \mu_{NAD}\ \mu_{NADH}\ \mu_{GLC}\ \mu_{PYR}\right)^T \tag{16.129}$$

$$\boldsymbol{V} = \left(v_{PGI}\ v_{PFK}\ v_{PGK}\ v_{PK}\ v_{HK}\right)^T \tag{16.130}$$

[13] NADH (reduced nicotinamide adenine dinucleotide) is an electron transporter within biomolecular processes [1].

The partitions of Y_d are

$$\boldsymbol{\mu}^D = \begin{pmatrix}\mu_{G6P} & \mu_{F6P} & \mu_{GAP} & \mu_{PEP}\end{pmatrix}^T \tag{16.131}$$

$$\dot{\boldsymbol{X}}^I = \begin{pmatrix}\dot{x}_{ATP} & \dot{x}_{ADP} & \dot{x}_{NAD} & \dot{x}_{NADH} & \dot{x}_{GLC} & \dot{x}_{PYR}\end{pmatrix}^T \tag{16.132}$$

$$\boldsymbol{V}^D = \begin{pmatrix}v_{PGI} & v_{PFK} & v_{PGK} & v_{PK}\end{pmatrix}^T \tag{16.133}$$

$$\boldsymbol{A}^I = \begin{pmatrix}A_{HK}\end{pmatrix}^T \tag{16.134}$$

and the partitions of U_d are

$$\dot{\boldsymbol{X}}^D = \begin{pmatrix}\dot{x}_{G6P} & \dot{x}_{F6P} & \dot{x}_{GAP} & \dot{x}_{PEP}\end{pmatrix}^T \tag{16.135}$$

$$\boldsymbol{\mu}^I = \begin{pmatrix}\mu_{ATP} & \mu_{ADP} & \mu_{NAD} & \mu_{NADH} & \mu_{GLC} & \mu_{PYR}\end{pmatrix}^T \tag{16.136}$$

$$\boldsymbol{A}^D = \begin{pmatrix}A_{PGI} & A_{PFK} & A_{PGK} & A_{PK}\end{pmatrix}^T \tag{16.137}$$

$$\boldsymbol{V}^I = \begin{pmatrix}v_{HK}\end{pmatrix}^T \tag{16.138}$$

The 15×15 matrix S_d summarised in Fig. 16.11d. The relevance of the submatrices S_{xx}, S_{AA}, $S_{A\mu}$ and S_{vv} are now examined in turn.

1. From the second row partition, S_{xx} has six zero-valued rows corresponding to the six chemostats *ATP*, *ADP*, *NAD*, *NADH*, *GLY* and *PYR*

$$\dot{x}_{ATP} = \dot{x}_{ADP} = \dot{x}_{NAD} = \dot{x}_{NADH} = \dot{x}_{GLY} = \dot{x}_{PYR} = 0 \tag{16.139}$$

   Unlike Example 16.4, there are no other conserved moieties in this open system.
2. From the fourth row partition

$$S_{AA} = \begin{pmatrix}-1 & -1 & -2 & -2\end{pmatrix} \tag{16.140}$$

$$\text{and } S_{A\mu} = \begin{pmatrix}-2 & 2 & 2 & -2 & 1 & -2\end{pmatrix} \tag{16.141}$$

   S_{AA}, together with $S_{A\mu}$, corresponds to the sum of the affinities along the glycolytic pathway being equal to the weighted sum of the relevant chemostat potentials

$$\begin{aligned} A_{PGI} + A_{PFK} + 2A_{PGK} + 2A_{PK} =& \mu_{GLC} - 2\mu_{PYR} \\ & - 2(\mu_{ATP} - \mu_{ADP}) - 2(\mu_{NADH} - \mu_{NAD}) \end{aligned} \tag{16.142}$$

   The right-hand side of this equation must be positive for glycolysis to proceed; thus the difference of the chemical potential of *GLC* (μ_{GLC}) and twice that of *PYR* ($2\mu_{PYR}$) must be sufficient to drive the creation of *ATP* from *ADP* and *NADH* from *NAD*.

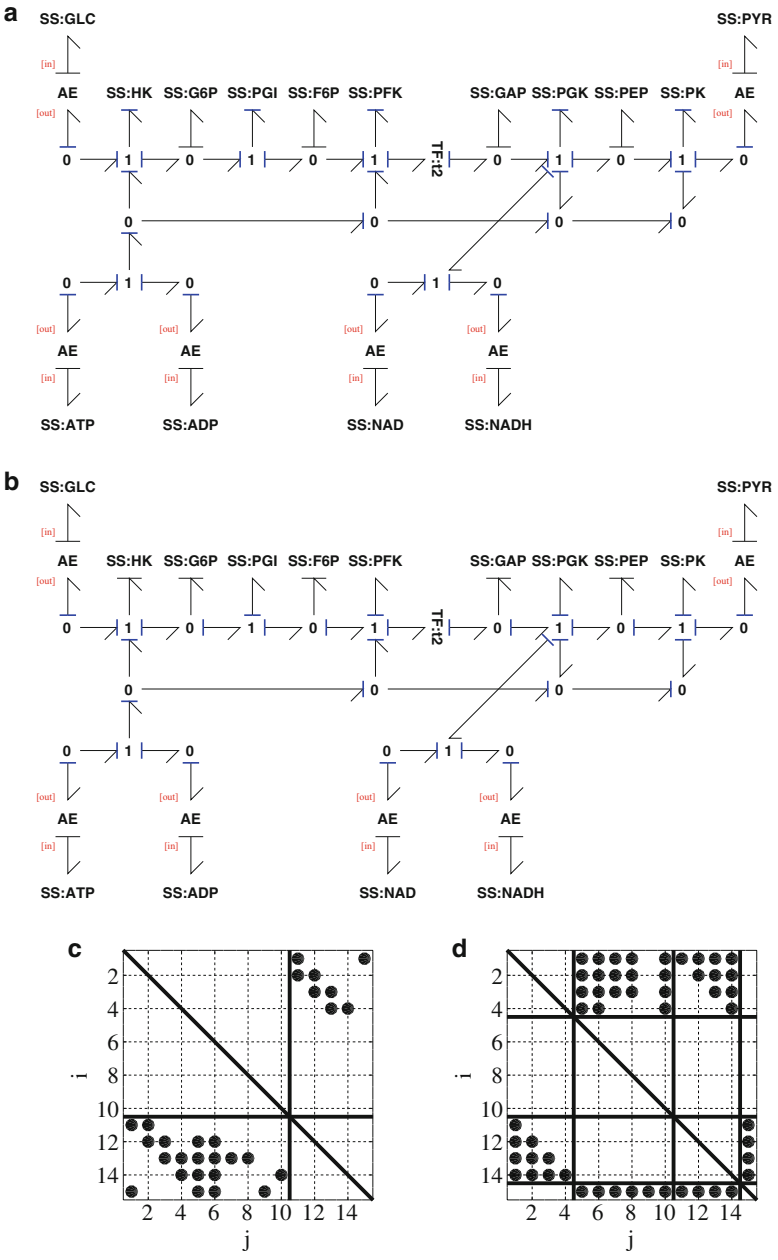

Fig. 16.11 Glycolysis. This simplified model of glycolysis corresponds to that of Cloutier et al. [8]. (**a**) System bond graph. (**b**) Junction structure with maximum derivative causality. (**c**) and (**d**) Alternative representation of the structure matrices S (16.43) and S_d (16.48) where *filled circle* indicates a non-zero entry and i and j the row and column indices respectively

3. From the third row partition

$$S_{vv} = \begin{pmatrix} 1 & 1 & 2 & 2 \end{pmatrix}^T \tag{16.143}$$

In the steady state ($\dot{\boldsymbol{X}} = 0$). In this case S_{vv} implies that, in the steady state, the reaction flows are related by

$$v_{PGI} = v_{PFK} = v_{HK} \text{ and } v_{PGK} = v_{PK} = 2v_{HK} \tag{16.144}$$

16.6 Example: Phosphorylation/Dephosphorylation

The phosphorylation/dephosphorylation reaction network is a standard building block of biomolecular systems. It is treated in detail by Beard and Qian [5, Sect. 5.1.1] and discussed by Gawthrop and Crampin [11, 12]. It comprises four reactions

$$\begin{aligned} M + ATP + E_1 &\overset{1}{\rightleftharpoons} C_1 & C_1 &\overset{2}{\rightleftharpoons} + ADP + MP + E_1 \\ MP + E_2 &\overset{3}{\rightleftharpoons} C_2 & C_2 &\overset{4}{\rightleftharpoons} M + P + E_2 \end{aligned} \tag{16.145}$$

In this example there are three chemostats corresponding to ATP, ADP and P; these act as the driver of the system.

The bond graph junction structure representation is given in Fig. 16.12b which is shown with derivative causality. The corresponding structure matrices S and S_d can be visualised using Fig. 16.12c, d. Note that the last three rows of N^{cd} correspond to the three chemostats and are zero.

The partitions of Y_d are

$$\boldsymbol{\mu}^D = \begin{pmatrix} \mu_{C1} & \mu_{C2} & \mu_{MP} \end{pmatrix}^T \tag{16.146}$$

$$\dot{\boldsymbol{X}}^I = \begin{pmatrix} \dot{x}_{E1} & \dot{x}_{E2} & \dot{x}_M & \dot{x}_{ATP} & \dot{x}_{ADP} & \dot{x}_P \end{pmatrix}^T \tag{16.147}$$

$$\boldsymbol{V}^D = \begin{pmatrix} v_1 & v_2 & v_3 \end{pmatrix}^T \tag{16.148}$$

$$\boldsymbol{A}^I = A_4 \tag{16.149}$$

and the partitions of U_d are

$$\dot{\boldsymbol{X}}^D = \begin{pmatrix} \dot{x}_{C1} & \dot{x}_{C2} & \dot{x}_{MP} \end{pmatrix}^T \tag{16.150}$$

$$\boldsymbol{\mu}^I = \begin{pmatrix} \mu_{E1} & \mu_{E2} & \mu_M & \mu_{ATP} & \mu_{ADP} & \mu_P \end{pmatrix}^T \tag{16.151}$$

$$\boldsymbol{A}^D = \begin{pmatrix} A_1 & A_2 & A_3 \end{pmatrix}^T \tag{16.152}$$

$$\boldsymbol{V}^I = v_4 \tag{16.153}$$

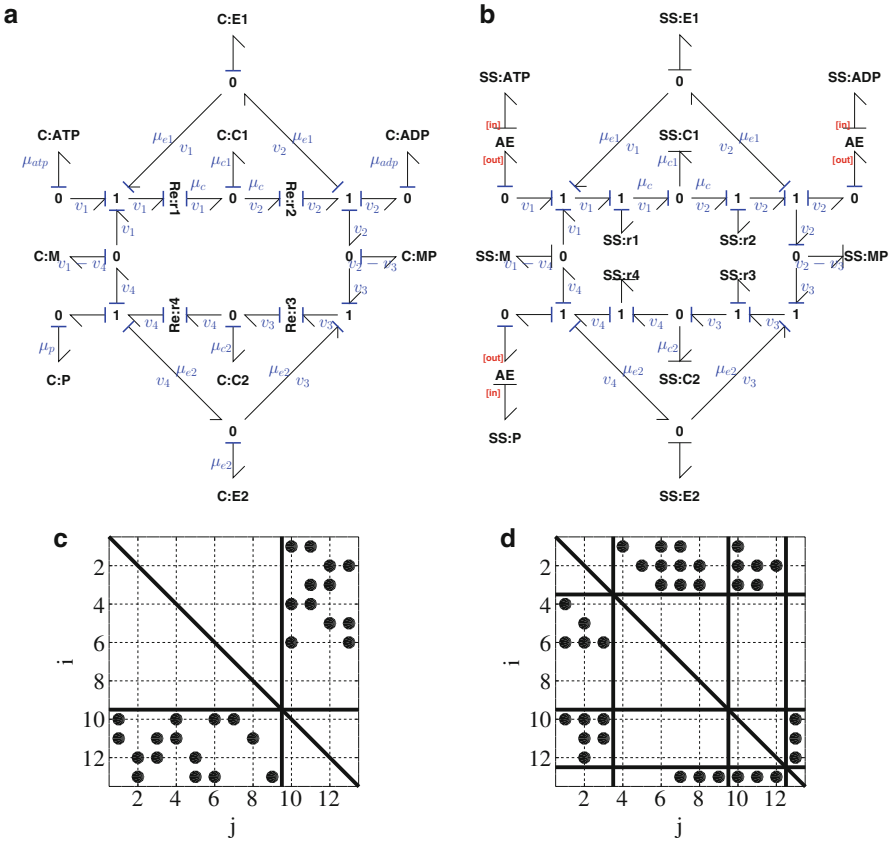

Fig. 16.12 Phosphorylation/dephosphorylation. This example is taken from Beard and Qian [5] and shows how driven by *ATP* hydrolysis, *M* is phosphorylated to *MP*, and *MP* dephosphorylated to *M*. (**a**) System bond graph. (**b**) Junction structure with maximum derivative causality. (**c**) and (**d**) Alternative representation of the structure matrices *S* (16.43) and S_d (16.48) where *filled circle* indicates a non-zero entry and *i* and *j* the row and column indices respectively

The 13×13 matrix S_d is summarised in Fig. 16.12d. The relevance of the submatrices S_{xx}, S_{AA}, $S_{A\mu}$ and S_{vv} are now examined in turn.

1. From the second row partition

$$S_{xx} = \begin{pmatrix} -1 & 0 & 0 \\ 0 & -1 & 0 \\ -1 & -1 & -1 \\ 0 & 0 & 0 \\ 0 & 0 & 0 \\ 0 & 0 & 0 \end{pmatrix} \tag{16.154}$$

the first and second rows of S_{xx} correspond to the conserved moieties $x_{e1} + x_{c1} = x_{\text{tot1}}$ and $x_{e2} + x_{c2} = x_{\text{tot2}}$. The third row of S_{xx} corresponds to the conserved moiety $x_{mp} + x_{c1} + x_{c2} + x_m = x_{\text{tot}}$. The fourth, fifth and sixth rows of S_{xx} correspond to the three constant chemostat states: x_{ATP}, x_{ADP} and x_P.

$$\dot{x}_{ATP} = \dot{x}_{ADP} = \dot{x}_P = 0 \tag{16.155}$$

2. From the fourth row partition

$$S_{AA} = \begin{pmatrix} -1 & -1 & -1 \end{pmatrix} \qquad \text{and} \qquad S_{A\mu} = \begin{pmatrix} 0 & 0 & 0 & 1 & -1 & -1 \end{pmatrix} \tag{16.156}$$

the first row of S_{AA}, together with the first row of $S_{A\mu}$, corresponds to the sum of the affinities around the central loop being equal to the weighted sum of the chemostat potentials

$$A_1 + A_2 + A_3 + A_4 = \mu_{ATP} - \mu_{ADP} - \mu_P \tag{16.157}$$

Thus the flow around the loop comprising $r_1 \ldots r_4$ is driven by the $ATP \rightleftharpoons ADP + P$ reaction.

3. From the third row partition

$$S_{vv} = \begin{pmatrix} 1 \\ 1 \\ 1 \end{pmatrix} \tag{16.158}$$

In the steady state ($\dot{\boldsymbol{X}} = 0$). In this case S_{vv} corresponds to the four reaction flows being equal

$$v_1 = v_2 = v_3 = v_4 \tag{16.159}$$

16.7 Conclusion

The causal properties of the bond graph junctions structures representing biomolecular systems have been examined and shown to provide an alternative approach to generating the related stoichiometric matrices. As a graphical approach, the bond graph method gives more intuitive insight than purely numerical approaches.

The bond graph approach uses causality arguments and the sequential causality assignment procedure (SCAP); the numerical approach uses Gaussian elimination. It follows that the bond graph approach must, in some sense, be equivalent to the Gaussian elimination approach; this deserves further investigation.

As discussed in this chapter, it can be more convenient to represent reactions by a one-port **R** component and associated **1** junction rather than a two-port **Re**

component. This raises the question as to whether it is always possible to model in this way. The key issue here is under what circumstances forward and reverse stoichiometric matrices N^f and N^r can be deduced from the stoichiometric matrix $N = N^r - N^f$.

This chapter focuses on turning closed biomolecular systems into open systems using the *chemostat* (constant chemical potential) concept previously used by Polettini and Esposito [35] and Gawthrop and Crampin [12]. It would be interesting to examine the use of the dual concept of *flowstats* (constant molar flow) [12] in the context of this chapter.

Gawthrop et al. [13] use *hierarchical* bond graph models to allow large models to be built out of submodels and use the notion of a *port* component to do this. It would be interesting to develop a hierarchical version of the methods presented in this chapter.

Acknowledgements Peter Gawthrop would like to thank the Melbourne School of Engineering for its support via a Professorial Fellowship. He would also like to thank Michael Pan and Joe Cursons for their close reading of the draft chapter.

References

1. Alberts, B., Johnson, A., Lewis, J., Morgan, D., Raff, M., Roberts, K., et al. (Eds.). (2015). *Molecular biology of the cell* (6th ed.). Abingdon: Garland Science.
2. Alon, U. (2007). *Introduction to systems biology: Design principles of biological networks*. Boca Raton: CRC Press.
3. Atkins, P., & de Paula, J. (2011). *Physical chemistry for the life sciences* (2nd ed.). Oxford: Oxford University Press.
4. Beard, D. A. (2012). *Biosimulation: Simulation of living systems*. Cambridge: Cambridge University Press. ISBN: 978-0-521-76823-8.
5. Beard, D. A., & Qian, H. (2010). *Chemical biophysics: Quantitative analysis of cellular systems*. Cambridge: Cambridge University Press.
6. Breedveld, P. C. (1982). Thermodynamic bond graphs and the problem of thermal inertance. *Journal of the Franklin Institute, 314*(1), 15–40. ISSN: 0016-0032. doi:10.1016/0016-0032(82)90050-3.
7. Cellier, F. E. (1991). *Continuous system modelling*. New York: Springer.
8. Cloutier, M., Bolger, F. B., Lowry J. P., & Wellstead P. (2009). An integrative dynamic model of brain energy metabolism using in vivo neurochemical measurements. *Journal of Computational Neuroscience, 27*(3), 391–414. ISSN: 0929-5313. doi:10.1007/s10827-009-0152-8.
9. Fuchs, H. U. (1996). *The dynamics of heat*. New York: Springer.
10. Gawthrop, P. J., & Bevan, G. P. (2007). Bond-graph modeling: A tutorial introduction for control engineers. *IEEE Control Systems Magazine, 27*(2), 24–45. doi:10.1109/MCS.2007.338279.
11. Gawthrop, P. J., & Crampin, E. J. (2014). Energy-based analysis of biochemical cycles using bond graphs. *Proceedings of the Royal Society A: Mathematical, Physical and Engineering Science, 470*(2171), 1–25. doi:10.1098/rspa.2014.0459. Available at arXiv:1406.2447.
12. Gawthrop, P. J., & Crampin, E. J. (2016). Modular bond-graph modelling and analysis of biomolecular systems. *IET Systems Biology, 10*, 2016. ISSN: 1751-8849. doi:10.1049/iet-syb.2015.0083. Available at arXiv:1511.06482.

13. Gawthrop, P. J., Cursons, J., & Crampin, E. J. (2015). Hierarchical bond graph modelling of biochemical networks. *Proceedings of the Royal Society A: Mathematical, Physical and Engineering Sciences, 471*(2184), 1–23. ISSN: 1364-5021. doi:10.1098/rspa.2015.0642. Available at arXiv:1503.01814.
14. Gawthrop, P. J., & Smith, L. (1992). Causal augmentation of bond graphs with algebraic loops. *Journal of the Franklin Institute, 329*(2), 291–303. doi:10.1016/0016-0032(92)90035-F.
15. Gawthrop, P. J., & Smith, L. P. S. (1996). *Metamodelling: Bond graphs and dynamic systems*. Hemel Hempstead: Prentice Hall. ISBN: 0-13-489824-9.
16. Greifeneder, J., & Cellier, F. E. (2012). Modeling chemical reactions using bond graphs. In *Proceedings ICBGM12, 10th SCS International Conference on Bond Graph Modeling and Simulation, Genoa, Italy* (pp. 110–121).
17. Hill, T. L. (1989). *Free energy transduction and biochemical cycle kinetics*. New York: Springer.
18. Jamshidi, N., & Palsson, B. (2010). Mass action stoichiometric simulation models: Incorporating kinetics and regulation into stoichiometric models. *Biophysical Journal, 98*(2), 175–185. ISSN: 0006-3495. doi:10.1016/j.bpj.2009.09.064.
19. Job, G., & Herrmann, F. (2006). Chemical potential – A quantity in search of recognition. *European Journal of Physics, 27*(2), 353–371 (2006). doi:10.1088/0143-0807/27/2/018.
20. Karnopp, D. (1990). Bond graph models for electrochemical energy storage: Electrical, chemical and thermal effects. *Journal of the Franklin Institute, 327*(6), 983–992. ISSN: 0016-0032. doi:10.1016/0016-0032(90)90073-R.
21. Karnopp, D. C., Margolis, D. L., & Rosenberg, R. C. (2012). *System dynamics: Modeling, simulation, and control of mechatronic systems* (5th ed.). New York: Wiley. ISBN: 978-0470889084.
22. Klipp, E., Liebermeister, W., Wierling, C., Kowald, A., Lehrach, H., & Herwig, R. (2011). *Systems biology*. Weinheim: Wiley.
23. Lambeth, M. J., & Kushmerick, M. J. (2002). A computational model for glycogenolysis in skeletal muscle. *Annals of Biomedical Engineering, 30*(6), 808–827. ISSN: 0090-6964. doi:10.1114/1.1492813.
24. Maxwell, J. C. (1871). Remarks on the mathematical classification of physical quantities. *Proceedings London Mathematical Society, 3*, 224–233.
25. Mukherjee, A., Karmaker, R., & Samantaray, A. K. (2006). *Bond graph in modeling, simulation and fault identification*. New Delhi: I.K. International.
26. Ort, J. R., & Martens, H. R. (1973). The properties of bond graph junction structure matrices. *Journal of Dynamic Systems, Measurement, and Control, 95*, 362–367. ISSN: 0022-0434. doi:10.1115/1.3426736.
27. Oster, G., & Perelson, A. (1974). Chemical reaction networks. *IEEE Transactions on Circuits and Systems, 21*(6), 709–721. ISSN: 0098-4094. doi:10.1109/TCS.1974.1083946.
28. Oster, G., Perelson, A., & Katchalsky, A. (1971). Network thermodynamics. *Nature, 234*, 393–399. doi:10.1038/234393a0.
29. Oster, G. F., Perelson, A. S., & Katchalsky, A. (1973). Network thermodynamics: Dynamic modelling of biophysical systems. *Quarterly Reviews of Biophysics, 6*(01), 1–134 doi:10.1017/S0033583500000081.
30. Palsson, B. (2006). *Systems biology: Properties of reconstructed networks*. Cambridge: Cambridge University Press. ISBN: 0521859034.
31. Palsson, B. (2011). *Systems biology: Simulation of dynamic network states*. Cambridge: Cambridge University Press.
32. Paynter, H. M. (1961). *Analysis and design of engineering systems*. Cambridge: MIT Press.
33. Paynter, H. M. (1993). Preface. In J. J. Granda & F. E. Cellier (Eds.), *Proceedings of the International Conference On Bond Graph Modeling (ICBGM'93)*. Simulation Series, La Jolla, CA, USA, January 1993 (Vol. 25). Society for Computer Simulation. ISBN: 1-56555-019-6.
34. Perelson, A. S. (1975). Bond graph junction structures. *Journal of Dynamic Systems, Measurement, and Control, 97*, 189–195. ISSN: 0022-0434. doi:10.1115/1.3426901.

35. Polettini, M., & Esposito, M. (2014). Irreversible thermodynamics of open chemical networks. I. Emergent cycles and broken conservation laws. *The Journal of Chemical Physics, 141*(2), 024117 doi:10.1063/1.4886396.
36. Qian, H., & Beard, D. A. (2005). Thermodynamics of stoichiometric biochemical networks in living systems far from equilibrium. *Biophysical Chemistry, 114*(2–3), 213–220. ISSN: 0301-4622. doi:10.1016/j.bpc.2004.12.001.
37. Rosenberg, R. C., & Andry, A. N. (1979). Solvability of bond graph junction structures with loops. *IEEE Transactions on Circuits and Systems, 26*(2), 130–137. ISSN: 0098-4094. doi:10.1109/TCS.1979.1084615.
38. Sueur, C., & Dauphin-Tanguy, G. (1989). Structural controllability/observability of linear systems represented by bond graphs. *Journal of the Franklin Institute, 326*, 869–883.
39. Sueur, C., & Dauphin-Tanguy, G. (1991). Bond-graph approach for structural analysis of MIMO linear systems. *Journal of the Franklin Institute, 328*, 55–70.
40. Sueur, C., & Dauphin-Tanguy, G. (1997). Controllability indices for structured systems. *Linear Algebra and its Applications, 250*, 275–287.
41. Thoma, J. U., & Atlan, H. (1977). Network thermodynamics with entropy stripping. *Journal of the Franklin Institute, 303*(4), 319–328. ISSN: 0016-0032. doi:10.1016/0016-0032(77)90114-4.
42. Thoma, J. U., & Mocellin, G. (2006). *Simulation with entropy thermodynamics: Understanding matter and systems with bondgraphs*. Heidelberg: Springer. ISBN: 978-3-540-32798-1.
43. Van Rysselberghe, P. (1958). Reaction rates and affinities. *The Journal of Chemical Physics, 29*(3), 640–642. doi:10.1063/1.1744552.
44. Wellstead, P. E. (1979). *Introduction to physical system modelling*. Academic Press: New York.